Limnol. Oceanogr., 53(5), 2008, 1835–1852

A model of photosynthesis and photo-protection based on reaction center damage and repair

Oliver N. Ross, C. Mark Moore,[2] *and Dave J. Suggett*
Department of Biological Sciences, University of Essex, Wivenhoe Park, Colchester CO4 3SQ, United Kingdom

Hugh L. MacIntyre
Dauphin Island Sea Lab, 101 Bienville Boulevard, Dauphin Island, Alabama 36528

Richard J. Geider[1]
Department of Biological Sciences, University of Essex, Wivenhoe Park, Colchester CO4 3SQ, United Kingdom

Abstract

Phytoplankton photosynthesis under the rapidly fluctuating irradiance which results from turbulent mixing through the vertical light gradient is poorly understood. Ship-based measurements often apply the fast repetition rate fluorescence (FRRF) technique in situ or in vivo to gauge the physiological state of the phytoplankton community and infer some of the physical properties of the water column (such as mixing time scales). We describe the development and validation of a model of photosynthetic electron turnover at photosystem II with consideration of downstream limitation, based on the redox state of photosystem II. We also include empirical formulations for slower processes such as photo-protection (from nonphotochemical quenching) and photo-inhibition. By confronting the simple model with laboratory data for *Dunaliella tertiolecta*, we were able to refine the model so that it faithfully produced rates of photosynthetic electron transfer determined by FRR fluorescence. Further, we were able to validate the model estimates of linear photosynthetic electron transfer rates against completely independent measurements obtained using ^{14}C-bicarbonate assimilation in photosynthesis-light curves.

The light dependence of phytoplankton photosynthesis is one of the most intensively studied aspects of phytoplankton physiology (Jassby and Platt 1976; Cullen 1990; Falkowski and Raven 2007). Nonetheless, most commonly used incubation procedures (e.g., Knap et al. [1996] p. 159) do not resolve photosynthesis rates on the time scales of variability in photon flux density (PFD) that are experienced by the phytoplankton in situ. It has long been recognized that variability in the light environment due to vertical mixing can affect the accuracy of estimates of in situ photosynthesis (Marra 1980; MacIntyre et al. 2000). Higher frequency variability, such as that caused by wave-focusing in the upper euphotic zone (Dera and Gordon 1970), does not appear to affect photosynthetic physiology in those eukaryotes studied (Stramski et al. 1993; Mouget et al. 1995*a*, *b*) but has been shown to induce an acclimative change in a cyanobacterium (MacKenzie and Campbell 2005). Numerous approaches have been made to mimic variability in the light regime in incubation experiments. These include manual (Yoder and Bishop 1985; Randall and Day 1987) or automated (Kirkpatrick et al. 1990; Gocke and Lenz 2004) movement of incubation bottles through the water column; circulation of the sample through a light gradient in a deck incubator (Jewson and Wood 1975; Gallegos et al. 1977); and imposing variable attenuation on a static sample through mechanical rotation of multiple filters (Mallin and Paerl 1992; Bertoni and Balseiro 2005).

Empirical approaches may fail to match the variability (both magnitude and frequency) imposed by the experimenter in the incubation to the variability that is experienced by phytoplankton in the natural environment. Accurately reproducing the natural light regime requires a priori knowledge of both the dynamic range and rate of change of irradiance. These can be derived from three parameters (the attenuation coefficient, the depth of the mixed layer, and the vertical diffusivity) for deck incubations and two (mixed-layer depth and diffusivity) for in situ incubations. Each of these input variables can vary within the duration of an hours-long incubation. Methods that have been tested or proposed for providing a match between the natural variability and the imposed regime include analysis of dye diffusion (Mallin and Paerl 1992), incorporation of motion sensors on a submersible incubator (Kirkpatrick et al. 1990) and parallel estimation of diffusivity, using an acoustic Doppler current profiler (Bertoni and Balseiro 2005). Incubations that use submerged samples account for changes in both the magnitude and spectral dependence of the attenuation coefficient. This is not the case for deck incubations, in which the use of filters with fixed optical characteristics imposes a defined

[1] Present address: National Oceanography Centre, University of Southampton, Southampton SO14 3ZH, United Kingdom.
[2] Corresponding author (geider@essex.ac.uk).

Acknowledgments

ONR and RJG gratefully acknowledge financial support from the MarQUEST initiative as part of the Natural Environment Research Council funded QUEST consortium. DJS and CMM were supported by Natural Environment Research Council postdoctoral fellowships. HLM was supported by National Science Foundation grant OCE-9907702. We are also grateful to K. Oxborough for useful discussions of the manuscript and to M. Behrenfeld for providing a helpful and thorough review.

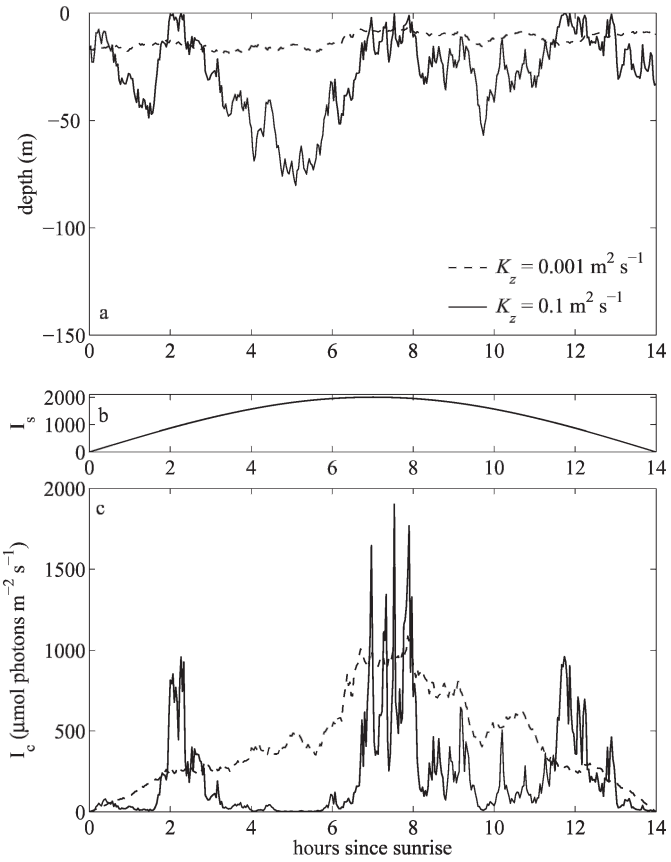

Fig. 1. Example PFD variability experienced in a 150-m surface mixed layer for two different vertical turbulent diffusivities K_z, using the random walk method from Ross and Sharples (2004). (a) shows an example particle trajectory in the SML for a low- and high-diffusivity scenario. (b) shows the sinusoidal variation of irradiance incident upon the sea surface, and (c) the light received by the cells at the depths shown in (a).

but invariable light spectrum. Last, both in situ and deck incubations employ end-point measurements, which provide the integrated production over the incubation period; thus, they do not resolve the time dependence of the productivity. Uncertainty in estimates of primary productivity due to vertical mixing is likely to be greatest when phytoplankton are mixed through large light gradients. Such conditions exist in a pre-spring bloom scenario in a temperate shelf sea and in estuaries, for instance, where strong vertical mixing due to tidal and wind-induced turbulence rapidly cycles the phytoplankton through the entire water column.

Figure 1 shows two example trajectories including the associated light variability experienced by cells in two different turbulence regimes in a modeled oceanic water column. These results were obtained from a Lagrangian random walk model applied to a fully mixed surface layer using the method described in Ross and Sharples (2004) and the exponential light absorption from Beer–Lambert's Law (e.g., Ross and Sharples 2007) with an absorption coefficient of 0.09 m^{-1}. In the low-turbulence case, the light received by the cells simply mimics the semidiurnal variation of the solar irradiance incident upon the sea surface because the vertical displacement of the cells is slow. In contrast, cells that are subject to a highly turbulent oceanic environment can travel from complete darkness to near-surface irradiance levels and back within just 1 h. Cells in estuarine water columns, where attenuation is higher and the mixed depth shallower by an order of magnitude or more, can undergo the same transition in 10 min or less (MacIntyre et al. 2000).

Primary productivity is commonly calculated from light response curves using bio-optical formalisms (Platt et al. 1980). Under these 'static' experimental conditions, the effects of photo-inhibition may be overestimated in surface waters and underestimated in deeper waters, with the errors depending on the time scales of photo-protection, photo-inhibition, and the turbulent displacement through the light gradient (Lewis et al. 1984).

The photosynthesis-light (P-I) response curve, or parameterizations that can be reformulated in terms of a P-I curve, are commonly used in bio-optical calculations of primary productivity. The parameters of the P-I curve are typically treated as 'constants' in models used to compute primary productivity. However, time-series observations over varying incubation times often show that these parameters are not constant (Marra 1980; MacIntyre et al. 2002). Furthermore, the light dependence of photosynthesis often differs in rising and falling light regimes (MacIntyre et al. 2000). Variability in the light dependence of biomass-specific photosynthesis in fluctuating light can result from the interaction of photo-protection, photo-inhibition, and photo-acclimation on discrete and/or overlapping time scales (Harris 1978; Geider et al. 1998).

Phytoplankton possess various mechanisms for coping with the wide range of PFDs to which they are exposed in nature (Harris 1978; Raven and Geider 2003). These include photo-protective mechanisms that either redirect excitation energy away from photosystem II (state transitions) or quench excitation energy to heat (Falkowski and Raven 2007) and photo-acclimation via changes in cellular pigment contents and, thus, light harvesting, operating on longer time scales (Geider et al. 1996). When photo-protection and photo-acclimation fail to provide adequate protection, photo-inactivation of photosynthesis may occur (Long et al. 1994).

It has been a long-standing goal of research in phytoplankton ecophysiology to be able to describe and predict the response of phytoplankton to fluctuating light (Cullen and Lewis 1988). Of particular interest is developing a predictive understanding of the response to vertical mixing (Lewis et al. 1984). The conceptual basis for this understanding is clear: the time scale for PFD fluctuations associated with vertical mixing depends on the depth of the mixed layer, the light attenuation coefficient, and the rate of vertical displacement through the resulting light gradient. Nondimensional solutions to simple reaction–diffusion equations describing phytoplankton responses to mixing have been developed (Lewis et al. 1984), although there are still open questions regarding the effect of turbulence and its effectiveness at mixing phytoplankton through vertical light gradients (Huisman and Sommeijer 2002).

Because ocean observation systems will never be capable of capturing the spatial and temporal heterogeneity of the planktonic ecosystem in its entirety, numerical models have been recognized as a valuable supplement to fill this observational gap. In the past, most photosynthesis models were empirical best-fit algorithms applied to experimental data sets (Steele 1962; Platt et al. 1980). An increasing demand by large-scale ecological and biogeochemical modelers for better representations of the phytoplankton physiology under realistic physical conditions has led to the advent of models with semiempirical to mechanistic descriptions of photosynthesis (Zonneveld 1997; Geider et al. 1998; Han 2002) and more realistic representations of turbulent mixing in coupled biological–physical models (Ross and Sharples 2007).

Our ultimate aim is to combine both approaches (i.e., to develop a mechanistic photosynthesis model that can explain the interaction between fluorescence, photosynthesis, photo-inhibition, photo-protection, and photo-acclimation at all PFDs and time scales, and to combine this biological model with a Lagrangian turbulence model where realistic physical forcing drives the vertically heterogeneous turbulent mixing). As a first step in this process, we present a model based on light absorption and photochemistry within photosystem II (PSII). As such, it is suitable for use in interpreting and exploiting the data generated by fast repetition rate (FRR) fluorescence (Kolber et al. 1998; Suggett et al. 2004). Our model is similar to that of Han (2002) who developed a model of photo-inhibition based on damage to PSII. However, the current model differs from previous formulations (Han 2002) in two important respects. First, it includes a downstream 'sink' limitation (e.g., limitations on the rates of inorganic carbon fixation and nitrate reduction). Second it includes photo-protection associated with the light-dependent reduction in the functional cross-section of PSII. The model allows us to simulate the time-dependence of photosynthesis under specified light regimes, including conventional P-I response curves. Model state variables, or proxies for these variables, can be measured by biophysical techniques including FRR fluorescence. Model parameters can be derived from experiments. We calibrated the model with PI curves for photosynthetic electron transfer rate obtained from experiments with the chlorophyte *Dunaliella tertiolecta*. We then validated the model against independent measurements of PI curves obtained from ^{14}C assimilation. To our knowledge, this is the first study in which an attempt is made to confront this type of model with experimental data.

Background to model structure

Recently, fluorescence techniques such as fast repetition rate (FRR) fluorescence have been used to determine the rate of photosynthetic electron transfer in marine phytoplankton (Kolber et al. 1998). These techniques use variable fluorescence that arises from photosystem II (PSII) to calculate the rate of linear electron transfer from water to nicotinamide adenine dinucleotide phosphate-oxidase (NADPH), where the electron transfer reactions within and beyond PSII have been summarized by Falkowski and Raven (2007). Linear electron transfer relies on use of a photon absorbed by PSII to photochemically oxidize a reaction-center chlorophyll, designated P680. The electron that is extracted from P680 is very rapidly (about 20 ps) transferred to a quinone, designated Q_A. Oxidized Q_A is a fluorescence quencher. The changes in fluorescence associated with the dynamics of the reduction and oxidation of Q_A can be used to investigate photosynthetic transfer at PSII. Reoxidation of Q_A^- occurs when it passes its electron to a second quinone, Q_B. When Q_B is oxidized, this transfer occurs with an e-folding time of reduced Q_A of about 400 μs (Falkowski and Raven 2007).

$$Q_A^- + Q_B \xrightarrow{\text{reoxidation of } Q_A^-} Q_A + Q_B^- \qquad (1)$$

with

$$\frac{1}{Q_A^-}\frac{\mathrm{d}Q_A^-}{\mathrm{d}t} = \exp\left(-\frac{t}{400}\right) \text{ where } t \text{ is in } \mu\text{s}. \qquad (2)$$

Once Q_B has been doubly reduced, it is protonated and becomes part of the plastoquinol pool. The plastoquinol pool is subsequently reoxidized by transfer of electrons to the cytochrome b_6:f complex and ultimately to NADPH following a second photochemical reaction in photosystem I. Plastoquinone is the oxidized form of plastoquinol.

Many features of variable fluorescence, and its relationship to linear electron transfer, can be explained using a model of the photosynthetic electron transfer chain. For example, Kroon and Thoms (2006) have recently presented a model of photosynthetic electron transfer in chlorophytes that explicitly considers the entire reaction sequence from Q_A to NADPH. The model includes 31 state variables and 29 rate constants. It can simulate the types of signals generated by FRR and other fluorescence techniques.

We consider a much simpler model in which the only state variable of the photosynthetic electron transfer chain is Q_A, and the reoxidation of reduced Q_A is characterized by two time constants. The rate of Q_A reduction is determined by the rate of photon absorption by PSII and the efficiencies of exciton transfer to, and charge separation within the PSII reaction center (RCII). We assume that under low-light conditions when the pool of Q_A^- is small compared with the pool of oxidized plastoquinone, Q_A^- will be reoxidized with a time constant determined by the maximum rate allowed by the kinetics of electron transfer to Q_B. However, under high-light conditions when the reduced plastoquinol pool becomes large, the rate of reoxidation of plastoquinol will become the limiting step, and the rate constant for reoxidation of Q_A^- will be increased (Sukenik et al. 1987; Behrenfeld et al. 1998; Falkowski and Raven 2007). Graphically, we represent this description of electron transfer in Fig. 2.

Although Kroon and Thoms (2006) provide a complete model of the photosynthetic electron transfer chain, the model does not include important processes that can modify the rate of photosynthetic transfer. Amongst these processes is nonphotochemical quenching, which is thought to play a role in protecting PSII reaction centers from

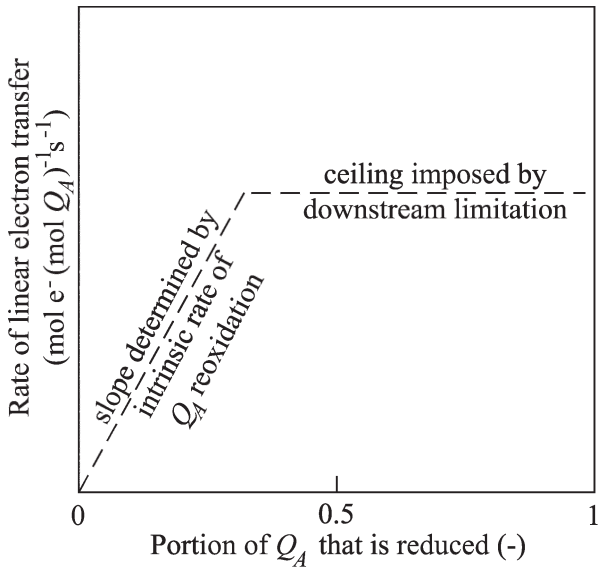

Fig. 2. Hypothesized dependence of the rate of linear electron transfer on the redox state of Q_A, which is the primary electron acceptor of reaction center II. The rate of linear electron transfer (ETR) is calculated in the model using Eq. 9 in Table 2. The proportion of the Q_A^a, that is reduced is given in the model by $Q_A^{red} : Q_A^a$.

photo-inhibition by reducing the efficiency of transfer of excitation energy from light-harvesting pigments to reaction center chlorophyll. We do not treat nonphotochemical quenching mechanistically. Rather, we adopt a pragmatic approach and develop a parameterization of nonphotochemical quenching that is assumed to be driven by the redox state of the Q_A pool.

Model structure

The model consists of a series of coupled differential equations which represent the main photochemical reactions on time scales that are important for the photophysiology of the cell. In the following description of the model structure, we have divided these equations into what we will call the 'fast' and the 'slow' reactions. The fast reactions occur on timescales that are much shorter than the relevant oceanic timescales governing the variability in the photon flux density incident upon a cell. These fast reactions are photochemical and will effectively equilibrate almost immediately to the ambient light environment at their steady state. The slow reactions occur on timescales which are comparable to or longer than those that govern the light variability. Because we anticipate that this model will be combined with a Lagrangian turbulence model, we present the slow reactions in a discretised form which is more amenable to this purpose. The model equations and main variables and units are summarized in Table 1 and 2.

General set-up—As in previous mechanistic model formulations (Eilers and Peeters 1988; Zonneveld 1997; Han 2002) we assume that at any one time, the photosystem can be found in one of the following three states: (1) oxidized (open), (2) reduced (closed), or (3) inhibited (damaged). The amount of reaction centers (per unit carbon) in each state shall be denoted with Q_A^{ox}, Q_A^{red}, and Q_A^i respectively (see Fig. 3). While reaction centers in the oxidized and reduced states can be considered active (i.e., they take part in the photochemical reactions), the inhibited centers are inactive and need to be repaired before they become available for photosynthesis again. The amount of active centers is thus $Q_A^a = Q_A^{ox} + Q_A^{red}$ and the total centers $Q_A^T = Q_A^{ox} + Q_A^{red} + Q_A^i$.

The redox reactions which determine the balance between Q_A^{ox} and Q_A^{red} have time scales of the order of

Table 1. Summary of symbols used for measured variables and model parameters.

Symbol	Description	Value or unit
C	Cellular carbon	mol or g C
$ETR_Q^{\max}$	Max. linear electron transfer rate through RCII set by downstream processes	mol e$^-$ (mol RCII s)$^{-1}$
$F_q' : F_v'$	Index of redox state of Q_A^a(=q_P)	dimensionless
I	Photon flux density	μmol photons m^{-2} s^{-1}
k_r	Repair rate coefficient	s^{-1}
k^*	Achieved reoxidation rate coefficient	s^{-1}
k_Q	Reoxidation rate from downstream limitation	s^{-1}
$k_Q^{\max}$	Max. (intrinsic) reoxidation rate	s^{-1}
Q_A^{ox}	No. of oxidized reaction centers	mol RCII (g C)$^{-1}$
Q_A^{red}	No. of reduced reaction centers	mol RCII (g C)$^{-1}$
Q_A^i	No. of inhibited reaction centers	mol RCII (g C)$^{-1}$
Q_A^a	No. of active reaction centers	mol RCII (g C)$^{-1}$
Q_A^T	Total No. of reaction centers	mol RCII (g C)$^{-1}$
Δt	Time step	s
β	Factor for photo-protection	dimensionless
Φ	Photosynthetic quotient	1.4–2 mol O_2 (mol CO_2)$^{-1}$
Φ_C	Ratio of CO_2 fixed to ETR	mol CO_2 (mol e$^-$)$^{-1}$
φ_{O_2}	Yield of O_2 per electron transferred through RCII	0.25 mol O_2 (mol e$^-$)$^{-1}$
φ_{PSII}	Quantum efficiency of charge separation at PSII	1 e$^-$ photon^{-1}
Θ	Chl *a*-to-carbon ratio	g Chl *a* (g C)$^{-1}$
σ	Absorption cross-section for PSII (dark acclimated cells)	m^2 (μmol photons)$^{-1}$
σ'	Effective absorption cross-section for PSII	m^2 (μmol photons)$^{-1}$
$\tilde{\sigma}'$	'Optimal' absorption cross-section	m^2 (μmol photons)$^{-1}$
τ_σ^i	Time constant for the induction of photo-protection	180 s
τ_σ^r	Time constant for the relaxation of photo-protection	s
Υ	Photosynthetic unit size	mol Chl *a* (mol RCII)$^{-1}$
Ψ_d	Damage probability	dimensionless

Table 2. List of model equations.

$\frac{dQ_A^{ox}}{dt} = -\sigma' \varphi_{PSII} I Q_A^{ox} + k^* Q_A^{red}$, with	(7a)
$Q_A^{ox} + Q_A^{red} = Q_A^a$	
$\frac{dQ_A^{red}}{dt} = \sigma' \varphi_{PSII} I Q_A^{ox} - k^* Q_A^{red}$	(7b)
with $k^* = \min\left\{ \begin{matrix} k_Q \\ k_Q^{\max} \end{matrix} \right.$, where $k_Q = ETR_Q^{\max} \frac{Q_A^T}{Q_A^{red} + Q_A^i}$	(7c)
Steady-state solutions: $\tilde{Q}_A^{ox} = \frac{k^* Q_A^a}{\sigma' \varphi_{PSII} I + k^*}$ and	(8)
$\tilde{Q}_A^{red} = \frac{\sigma' \varphi_{PSII} I Q_A^a}{\sigma' \varphi_{PSII} I + k^*}$	
$ETR_Q = \sigma' \varphi_{PSII} \frac{Q_A^{ox}}{Q_A^a} \frac{Q_A^a}{Q_A^T} I = \sigma' \varphi_{PSII} \frac{Q_A^{ox}}{Q_A^T} I$	(9)
$P^C = ETR_Q \frac{\varphi_{O_2}}{\Phi} Q_A^T = \sigma' \varphi_{PSII} \frac{\varphi_{O_2}}{\Phi} Q_A^{ox} I$	(10)
Photo-inhibition and -repair:	(11)
$(Q_A^i)_{n+1} = (Q_A^i)_n + (\Psi_d \sigma' I Q_A^{red} - k_r Q_A^i)\Delta t$	
Photo-protection: $\frac{\tilde{\sigma}'}{\sigma} = 1 - \beta\left(\frac{Q_A^{red} + Q_A^i}{Q_A^T}\right)$,	(12)
where $\beta = f(\Upsilon)$ (*see* text)	
Induction of photo-protection:	(13a)
$\sigma'_{n+1} = \sigma'_n + \frac{1}{\tau_\sigma^i}(\tilde{\sigma}'_n - \sigma'_n)\Delta t$	
Relaxation of photo-protection:	(13b)
$\sigma'_{n+1} = \sigma'_n + \frac{1}{\tau_\sigma^r}(\tilde{\sigma}'_n - \sigma'_n)\Delta t$	

1 ms (Falkowski and Raven 2007), several orders of magnitude faster than any relevant physical-mixing time scale in the ocean and, hence, we will refer to them as the 'fast reactions.' The reactions which determine the balance between damage and repair of reaction centers occur on comparatively longer timescales. Photo-protection is assumed to decrease the effective cross-section for photosystem II, whereas photo-inhibition involves the inactivation of PSII reaction centers. Although this part of the model has not yet been fully validated, we have included it here for the sake of completeness (*see* also the Discussion).

Fast reactions: Photosynthetic electron transfer is initiated in PSII, with the requirement that the light-driven reduction of the primary acceptor (e.g., the quinone Q_A) is balanced by its reoxidation (Eq. 7 in Table 2). The ratio of oxidized and reduced centers in the steady state is thus given by the ratio of the achieved turnover rate k^* and the rate of photon arrival $\sigma' I$ (Eq. 8; we assume that the quantum efficiency of charge separation in RCII $\phi_{PSII} = 1$). Equation 7 contains already one difference to previous formulations (Han 2002; Baklouti et al. 2006). Rather than assuming a constant turnover rate for the reoxidation reactions, we introduce a potential downstream limitation in the electron transport rate (ETR) given by the condition in Eq. 7c (*see* also Fig. 2). Under light-limiting conditions the reoxidation of Q_A^{red} occurs much faster than the rate of photon arrival (i.e., $k^* > \sigma' I$). Hence only few centers are in the reduced state (Q_A^{red} is small) and $k^* = k_Q^{\max}$ (note that $k_Q^{\max}$ corresponds to τ^{-1} in Han (2002) and Baklouti et al. [2006]). As the PFD increases and, thus, the rate of photon arrival $\sigma' I$ increases, Q_A^{red} will also increase. At some point k_Q will drop below $k_Q^{\max}$ and the downstream limitation comes into effect. This corresponds to light-saturating conditions where the reoxidation of Q_A^{red} is determined by the demand for reductant by CO_2 fixation, nitrate assimilation, and biosynthesis. Other processes that may allow reoxidation of Q_A^{red}, such as the Mehler reaction (Asada 2000) are not included in the model. Under these light-saturating conditions, the ETR through Q_A is at a maximum as indicated by the "ceiling" in Fig. 2. Essentially, this model includes one possible formulation of the "excess" PSII capacity identified by Behrenfeld et al. (1998). Photo-inhibition (*see* below) will lead to a reduction of active centers, Q_A^a, and therefore also a decline in the amount of Q_A^{red} which counteracts the downstream limitation (Behrenfeld et al. 1998).

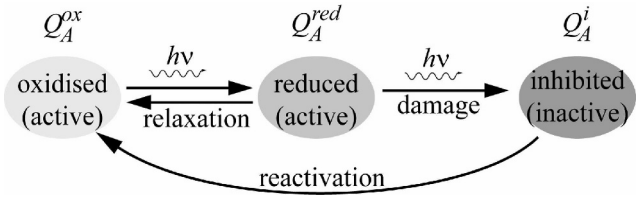

Fig. 3. Schematic representation of Eqs. 7 and 11 from Table 2.

The rate of linear electron transfer (ETR_Q) through PSII (Eq. 3, *see* below) is calculated in a manner that is directly analogous to calculations of ETR_Q using FRR fluorescence (Suggett et al. 2006). This facilitates calibration of the model based on FRR data and comparison of model outputs with FRR data.

We assume that the carbon-specific gross CO_2 fixation rate, P_C, is directly proportional to the product of ETR_Q and Q_A^T (Eq. 10), with the proportionality factor determined by the yield of O_2 per electron transferred through RCII, φ_{O_2}, and the photosynthetic quotient, Φ. This is a simplification because a number of processes may lead to uncoupling of CO_2 fixation from electron transfer through RCII, and the importance of these processes may differ amongst algal taxa (Wagner et al. 2006; Wilhelm et al. 2006). The photosynthetic quotient is determined by the biochemical composition (e.g., protein : lipid : carbohydrate) and nitrogen source (e.g., nitrate or ammonium) (Kroon and Thoms 2006).

Photo-inhibition and repair: All processes that we describe in this section occur on timescales which can be modeled explicitly with the currently available computing power of a standard desktop computer.

The slow reactions depicted in Fig. 3 are photo-inactivation (i.e., the transition from Q_A^{red} to Q_A^i) and the subsequent repair of RCII. Both processes have relevant timescales that are several orders of magnitude larger than those for the fast redox-reactions that determine the steady-state equilibrium between Q_A^{ox} and Q_A^{red} (Eq. 8). Net photo-inhibition is treated as the difference between the rates of damage and repair of PSII reaction centers (Eq. 11 in Table 2). Following Han (2002), we assume that the rate of

photo-inhibition is proportional to the rate of excitation energy transfer to Q_A^{red}, consistent with the mechanism suggested by Melis (1999). The steady state between Q_A^{ox} and Q_A^{red} is reached immediately at the beginning of a model time step Δt. At the end of the time step, some centers will have become inhibited, others repaired, and the number of active centers is adjusted accordingly as $(Q_A^a)_{n+1} = (Q_A^T - Q_A^i)_{n+1}$ for use in Eq. 8 during the next iteration.

Photo-protection: Photo-protection is assumed to operate by reducing the effective cross-section of PSII (σ'), thus accounting for the component of nonphotochemical quenching that is associated with processes that operate in the light-harvesting antenna. Photo-protection may also occur through nonphotochemical quenching in the reaction center (Gorbunov et al. 2001); however, this process is not currently included. In the model, antenna quenching is parameterized by requiring that σ' adjust to a value $\tilde{\sigma}'$ which depends on the ratio of oxidized to total reactions centers (Eq. 12) and a parameter β which depends on the acclimation state of the cell, represented by the photosynthetic unit size Υ.

We assume that the phytoplankton cell is not able to reach $\tilde{\sigma}'$ immediately. Instead, at each time step, the value $\tilde{\sigma}'$ is calculated from Eq. 12 and we then assume first-order kinetics to calculate the actual cross-section σ' (Eq. 13). σ' thus contains a cumulative account of the recent light-history of the cell. The time constants $\tau_\sigma^{i,r}$ can be determined from FRRF measurements. Note that we assume different time constants for transitions from low to high light (induction) and from high to low light (relaxation). This agrees with findings from Lohr and Wilhelm (2001) who found differences in rate constants for xanthophyll cycle pigment conversions in a diatom. Reported time-constants for xanthophyll de-epoxidation in the light are higher (i.e., faster) than those reported for epoxidation in the darkness, albeit in different microalgae (Olaizola et al. 1994; Goss et al. 2006) . If the nonphotochemical quenching is assumed to be due to the xanthophyll cycle, then the time constants for changes of σ' will differ as well.

Methods, results, and model evaluation

The FRRF experiments—In this section we calibrate and test the model against data obtained from laboratory FRR fluorescence measurements on the chlorophyte *Dunaliella tertiolecta*.

Cell growth: *Dunaliella tertiolecta* (strain CCMP 1320) was cultured under continuous illumination at three photon flux densities (PFD; 18, 80, and 300 μmol photons m^{-2} s^{-1}, provided by cool-white fluorescent lamps) and at constant temperature (20°C). We will refer to these cultures as the low-light (LL), mid-light (ML), and high-light (HL) cultures respectively. All cultures were grown in 'semi-batch' mode in artificial seawater (ASW; Keller et al. 1987) enriched with f/2 nutrients (Guillard and Ryther 1962). Cell growth was monitored from daily measurements of biomass as chlorophyll concentration and each alga was maintained and harvested in exponential growth phase.

Chlorophyll *a* and particulate organic carbon: The cultures used in this model were in exponential growth phase. For chlorophyll *a* (Chl *a*) analysis 1–5 ml of culture was filtered on to 25-mm Whatman GF/F glass fiber filters at low pressure (<5″ Hg or <16 kPa). Pigments were extracted for 15 min in darkness at room temperature in a 5-mL volume of 3:2 90% acetone:dimethyl sulfoxide (DMSO) (Shoaf and Lium 1976). Chl *a* was determined in a Turner TD-700 fluorometer using the nonacidification method (Welschmeyer 1994). The fluorometer was calibrated on pure Chl *a* (Sigma 25730), whose concentration was calculated from optical density via the coefficients in Jeffrey et al. (1997). For particulate organic carbon (POC), 50-mL samples were collected on Whatman GF/Fs that had been baked at 500°C for 2 h. After drying the filters, C and N were determined with an elemental analyzer (Costech CHN), using ethylene diamine tetraacetic acid (EDTA; Sigma 46081) as a standard.

FRR fluorometry and PSU size: A FAST*tracka* Fast Repetition Rate (FRR) fluorometer (Chelsea Technology) was programmed to deliver sequences that induce single-turnover (ST) saturation of PSII as described by Suggett et al. (2003, 2004). Between 10 and 20 individual ST sequences were averaged to reduce the random error associated with instrument noise (Suggett et al. 2004). A biophysical model describing ST saturation of PSII (Kolber et al. 1998) was then fitted to each averaged ST sequence to generate measures of minimum and maximum fluorescence yield and of PSII effective absorption, termed F_o (F'), F_m (F'_m), and σ_{PSII} (σ'_{PSII}) under dark-adapted (and actinic) light conditions. PSII photochemical efficiency was calculated as $(F_m - F_o) : F_m$ ($= F_v : F_m$) or $(F'_m - F') : F'_m$ ($= F_q' : F'_m$) under dark-adapted and actinic light conditions, respectively (*see* Suggett et al. 2003). Samples were dark-adapted for 1 h prior to fluorescence measurements to yield maximum values of $F_v : F_m$ (dimensionless) and of σ_{PSII} (m^2 μmol photons^{-1}). Each sample was then exposed to a gradient of actinic light between 5 and 1,250 μmol photons m^{-2} s^{-1} to characterize the light-response of PSII fluorescence (*see* Suggett et al. 2003). Actinic illumination was provided by quartz-halogen bulbs, attenuated through Lee neutral-density filters and filtered through a 2.5-cm layer of 10 g L^{-1} $CuSO_4$ (aq.). Each actinic PFD was delivered for a period of ~4 min followed by a dark period of 20 s (Fig. 4). ST sequences were averaged for the final 30 s of each actinic PFD treatment, by which time fluorescence yields had reached a steady state and for each dark period. All values of PSII effective absorption and actinic PFD were adjusted to the spectrum of light used for growth (Suggett et al. 2004).

The ratio of Chl *a* to functional RCII, which is often designated the photosynthetic unit size for PSII, (Υ, mol Chl *a* [mol RCII]$^{-1}$; Table 3) was determined from oxygen evolution during flash yield experiments. ST saturating flashes were provided at frequencies of 10 s^{-1} to 50 s^{-1} via a custom-built ST saturation flash system (as described in Suggett et al. 2003, 2004). Prior to measurement, samples were

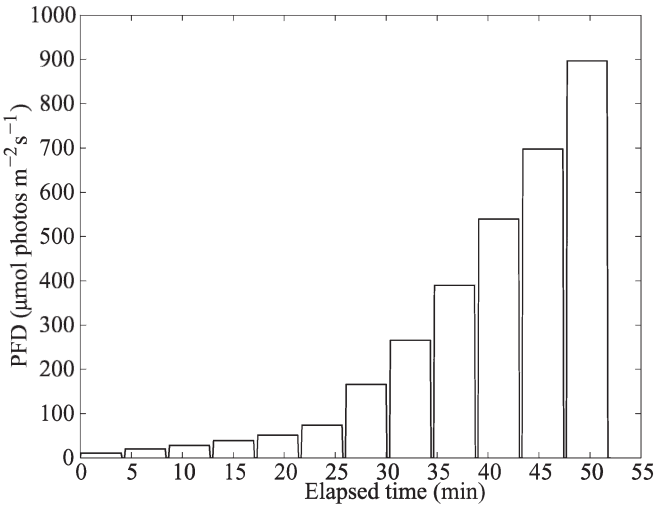

Fig. 4. Time course of the actinic photon flux density during the FRRF experiments. After every 4 min of light exposure, the cells are kept in the dark for 20 s to obtain measurements of σ'. Note that the ML and HL experiments reach slightly higher maximum PFDs of ~1,250 μmol photos m^2 s^{-1}.

gently concentrated by gravity filtration to provide the biomass necessary to yield the O_2 signal. Chl *a* was determined on 0.25 mL of concentrate as described above for unconcentrated samples. Calculation of Υ enabled determination of chlorophyll- and carbon-normalized electron transfer rates (ETR_x, μmol e$^-$ (g X)$^{-1}$ s^{-1}) for each PFD as

$$ETR_{Chl} = \frac{I\sigma'_{PSII}}{892}\frac{F'_q}{F'_v}\Upsilon^{-1} \quad (3a)$$

$$ETR_C = I\sigma'_{PSII}\frac{F'_q}{F'_v}\Upsilon^{-1}\cdot\Theta\cdot 1{,}120.5 \quad (3b)$$

where Θ is the Chl *a*-to-carbon ratio in units of g Chl *a* (g C)$^{-1}$, Υ is the photosynthetic unit size (mol Chl *a* [mol RCII]$^{-1}$) and the factor 1,120.5 accounts for the conversion of mol Chl *a* to g Chl *a* (892 gChl *a* [mol Chl *a*]$^{-1}$), mol RCII to μmol RCII and assumes 1 mol e$^-$ (mol RCII)$^{-1}$.

^{14}C uptake, light absorption—Photosynthesis-light (PI) response curves were determined for uptake of ^{14}C via incubations in a temperature-controlled photosynthetron (Lewis and Smith 1983), essentially as described by MacIntrye et al. (1996). Samples were illuminated for 40 min at PFDs between 10 and 1,700 μmol photons m^{-2} s^{-1} using quartz-halogen lamps, filtered through a 2.5-cm layer of 10 g L^{-1} $CuSO_4$ (aq.). Chlorophyll-specific and carbon-specific ^{14}C uptake rates were normalized to the Chl *a* and C concentrations measured in the initial sample.

Light-absorption coefficients were calculated from measurements of optical density on the concentrates of each sample using a U-3000 spectrophotometer fitted with an integrating sphere (ϕ60; Hitachi). Growth medium was used as a blank. Absorption was calculated from optical density after correcting for path length and residual scattering at 750 nm. An absorption coefficient was determined as the mean absorption between 400 and 750 nm normalized to Chl *a* concentration (a_{chl}, m^2 mg Chl a^{-1}).

Results and parameter estimation from the FRRF experiments—Table 3 summarizes the main parameters and characteristics for the three different cultures. The cultures show the typical pattern of acclimation of photosynthetic unit size (Υ) and the Chl *a*-to-carbon ratio (Θ) to growth at different PFDs. Both Υ and Θ decreased in response to growth at higher PFDs. However, the carbon-specific light-saturated electron transfer rate, $ETR_C^{\max}$, was largely independent of the growth PFD (cf. Fig. 5c) while Q_A^a declined by >56% between the lowest and highest growth PFDs (Table 3).

The carbon-specific initial slope of a plot of ETR_C vs. the fraction of the Q_a that is reduced, which we denote $k_C^{\max}$, was also found to be largely independent of the growth PFD (Fig. 5d), where $Q_A^{red}:Q_A^a$ was calculated as $1-(F'_q:F'_v)$. The numerical value for $k_C^{\max}$ was determined from a least-squares regression of the initial data points from the LL, ML, and HL experiments, yielding $k_C^{\max}$ = 156.5 μmol e$^-$ (g C)$^{-1}$ s^{-1} (r^2 = 0.75). The electron transfer rate ETR_C is equivalent to the rate of exciton arrival σIQ_A^{ox}:892$\Upsilon\Theta$ where we estimated Q_A^{ox} as $F'_q:F'_v$ (cf. Eq. 3). $ETR_C^{\max}$ was obtained by averaging the light-saturated values of ETR_C. for the LL and HL cultures yielding $ETR_C^{\max}$ = 15.75 μmol e$^-$ (g C)$^{-1}$ s^{-1}.

As the model is formulated on a reaction-center basis, we need to convert the above values from a carbon to a reaction-center basis. This was achieved by using the measured Q_A^a (mol RCII [mol C]$^{-1}$) from Table 3. The relationship between $ETR_Q^{\max}$ and $ETR_C^{\max}$ is

$$ETR_C^{\max} = ETR_Q^{\max}\cdot Q_A^a \quad (4)$$

The graphical result is shown in Fig. 5a and b and the numerical values for $k_Q^{\max}$ and $ETR_Q^{\max}$ which are used in Eq. 7c can be found in Table 3. Contrary to our expectation that $k_Q^{\max}$ would be independent of the acclimation state of the cells (*see* Fig. 2), we found that $k_Q^{\max}$ increased during acclimation to higher PFD (Fig. 5b) (Kaňa et al. 2002). The observed increase of $ETR_Q^{\max}$ with growth PFD is consistent with a decline in Q_A^a with growth PFD (Table 3) at constant $ETR_C^{\max}$ (Fig. 5c). In our model, we assumed that the rate of whole-chain linear electron transfer (and thus $ETR_C^{\max}$) is set by the rate of regeneration of $NADP^+$ and ADP by CO_2 fixation in the Calvin cycle, consistent with results reported previously for *D. tertiolecta* (Sukenik et al. 1987).

Model configuration and results—The model was initialized with the values of Υ, Θ, and σ' from Table 3 and forced with the time course of the PFDs from the FRRF measurements (cf. Fig. 4). $ETR_Q^{\max}$ and $k_Q^{\max}$ were determined from Fig. 5 as described in the previous section, and β was chosen such that the model would reproduce the amplitude of the maximum observed depression in $\sigma':\sigma$ due to photo-protection (*see* below). The overall sensitivity

Table 3. Main parameters for the low light (LL), medium light (ML), and high light (HL) FRRF experiments on *Dunaliella tertiolecta*. Values for σ have been spectrally corrected. *See* text on how ETR_Q^{max} and k_Q^{max} have been determined.

Experiment	LL	ML	HL
Growth irradiance I_g (μmol photons m^{-2} s^{-1})	18	80	300
Specific growth μ (d^{-1})	0.20	1.19	1.67
a_{CHL} (400–700 nm) (m^2 [g Chl a]$^{-1}$)	4.81	5.31	6.67
ETR_Q^{max} (mol e^- [mol RCII s]$^{-1}$)	121	159	280
$F_v : F_m$	0.55	0.51	0.53
k_Q^{max}(s^{-1})	1,215	1,595	2,805
Q_A^a(μmol RCII [mol C]$^{-1}$)	1.54	1.16	0.67
σ (m^2 [μmol photons]$^{-1}$)	0.945	0.87	0.65
$\sigma(\Upsilon a_{CHL})^{-1}(-)$	0.32	0.28	0.21
Θ (g Chl a [g C]$^{-1}$)	0.0849	0.0555	0.0247
Υ (mol Chl a [mol RCII]$^{-1}$)	741	638	498

of the model to changes in these parameters is discussed below. Considering that the model is a very simplified representation of the photochemical processes in PSII, the overall agreement between the model and the FRRF data is very good (Fig. 6). The model needed very little tuning in order to fit the data. In fact, the only two remaining parameters that were chosen freely are the photo-protection parameter β and the time constant τ_σ^i (cf. Table 1). The value of the latter determines how quickly the cell can activate photo-protective mechanisms in response to an excess in light availability.

In some respects, it is not surprising that we obtained good agreement between the model-derived ETR (Eq. 9) and the ETR obtained from FRR fluorescence (Eq. 3b) since the model was parameterized with the same FRR data as were used in Eq. 3b. What the model provides is a mechanism to account for the observations of the PFD dependencies of $F_q' : F_v'$ and σ' (Eqs. 8, 12, 13) obtained by FRR fluorescence during the generation of an ETR_Q vs. PFD curve.

One clear mismatch between our model and the observations can be seen in the ML data set (Fig. 6b), where the model overestimates Q_A^{ox} at intermediate PFDs of about 350–750 μmol photons m^{-2} s^{-1}. This discrepancy results from the way we have set up the model for this particular figure, using the same value of ETR_C for all three cultures. The high ETR_C values at intermediate PFDs in the ML culture appear to be anomalous when compared to the ETR_C values for the LL and HL cultures. We do not have an explanation for this anomalous behavior. Interestingly, this anomalous behavior is not evident when ETR_C is compared with CO_2 assimilation. We will return to this issue in the Discussion.

The magnitude of k_Q^{max} affects the balance between Q_A^{ox} and Q_A^{red} at a given PFD (Eq. 8) within the range where ETR is light-limited (i.e., where $k^* = k_Q^{max}$). At higher photon flux densities, the achieved reoxidation rate, k^*, is independent of k_Q^{max} as it is set by the downstream limitation (Fig. 6j–l). We found a linear relationship between the degree of photo-protection applied in the model, β (cf. Eq. 12), and the measured photosynthetic unit size Υ (Fig. 7)

$$\beta = c_1 \Upsilon + c_2 \quad (5)$$

At a given PFD, cells that were acclimated to low light showed a greater reduction in $\sigma' : \sigma$ than cells that were grown under higher light intensities (cf. Fig. 6). The value for τ_σ^i was chosen such that it would give a good representation of the $\sigma' : \sigma$ data in Fig. 6. The value that is used in Fig. 6 comes from the upper end of the range of possible values that deliver a good fit. Choosing a shorter time scale for the induction of photo-protection (τ_σ^i <180 s) will also produce good fits but larger values will not.

Model sensitivity—We test the sensitivity of the model by examining its response to 50% changes in the key model parameters. The first two, k_Q^{max} and ETR_Q^{max}, were determined directly from FRRF measurements (Fig. 5), while the third, β, had to be set during the tuning procedure. Both sources have uncertainties associated with them and this section aims to elucidate how these could affect the model behavior and to gauge how well these parameters are constrained.

The first parameter to be examined is k_Q^{max}. As mentioned previously, the magnitude of k_Q^{max} affects the balance between Q_A^{ox} and Q_A^{red} but only at low PFDs. This is shown for the example of the LL and HL cultures in Fig. 8. If we use a value for k_Q^{max} that is 50% below the one determined from Fig. 5, we find that the model slightly underestimates the amount of reaction centers in the oxidized state (dashed curve in Fig. 8a). Using a value for k_Q^{max} that is 50% above the chosen value, the effect is much smaller because most of the reaction centers will be in the oxidized state at low light intensities anyway. The ratio of $\sigma' : \sigma$ and ETR_Q^{max} (Fig. 8d, g) are essentially unaffected by a 50% change in k_Q^{max}.

In contrast, the model is much more sensitive to changes in ETR_Q^{max}. A 50% over- or underestimation leads to noticeable discrepancies between the model output and data (Fig. 8b, e, h). This value affects the amount of oxidized centers, Q_A^{ox}, which in turn affects the amount of photo-protection (cf. Eq. 12) and, therefore, also the point at which the downstream limitation comes into effect (Fig. 8k).

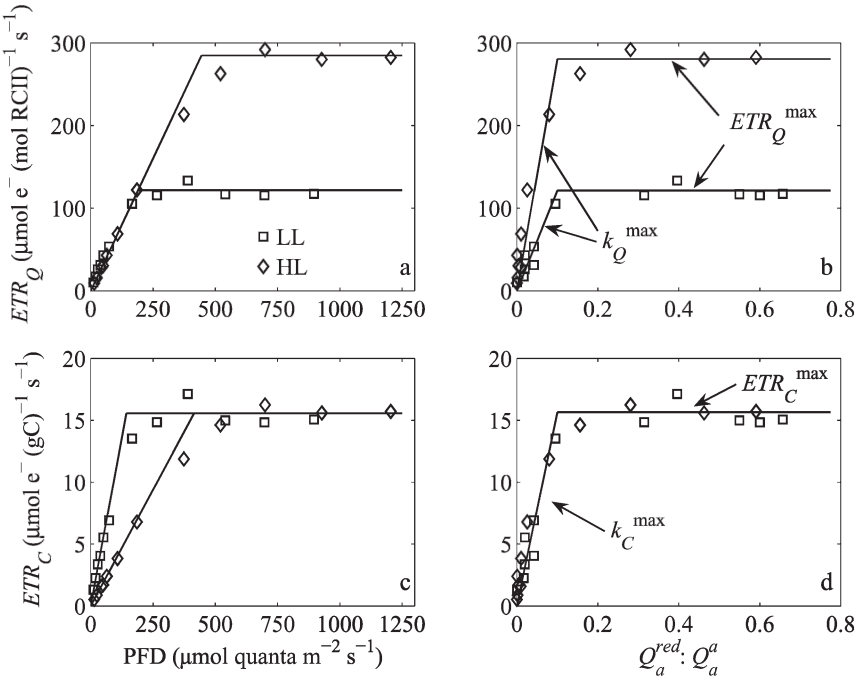

Fig. 5. Dependence of the (linear) electron transfer rate, $ETR_Q = \sigma' I F'_q{:}F'_v$ (a) on PFD and (b) on the proportion of the Q_A pool that is reduced. (c) and (d) show the corresponding plots on a carbon-specific basis instead of reaction center basis. The ML data have been omitted from this plot (but *see* Figs. 6b, 9).

The third parameter to be examined here is β, the magnitude of photo-protection. In the LL scenario, β is large, and a 50% change will lead to a significantly different model output for $Q_A^{ox}{:}Q_A^T$ (Fig. 8c). Since a lower (higher) $\sigma' : \sigma$ is matched by an equally higher (lower) ratio of $Q_A^{ox}{:}Q_A^T$, the net effect on ETR_Q is zero. In the HL scenario, β is rather small (0.25) and a 50% under- or overestimation will, therefore, have very little effect on the model.

Discussion

To date, FRR fluorescence has been used to calculate the rate of linear electron transfer. When used in situ, FRR fluorescence provides instantaneous (typically <1-s time resolution) point measurements of ETR. Extrapolation from these measurements to hourly or daily integrals requires either that the instrument be deployed continuously, or that the results be incorporated into a model. In some comparisons of FRR-based measurements of ETR with conventional measurements of ^{14}C assimilation, the implicit assumption has been that the instantaneous ETR also applies to longer time scales associated with the ^{14}C measurements (Kolber and Falkowski 1993). The most common model that can be used for extrapolation is a light-response curve with constant parameters, although other models such as those based on light absorption and the light dependence of quantum efficiency can be envisaged (Smyth et al. 2004; Suggett et al. 2006). In contrast to these empirical approaches, we have used a simple mechanistic model of PSII photochemistry to interpret FRR fluorescence data.

In this paper, our strategy has been to model explicitly the proportions of the Q_A^T pool that are oxidized and reduced (Eqs. 7a–c and 10). We have chosen to use a very simple representation of the PSII functioning (as depicted in Fig. 2). One advantage of this approach is that it minimizes the number of parameters that need to be specified. Another advantage is that these parameters can be measured directly by FRR fluorescence. To these fast reactions, we have added empirical descriptions of photoinhibition (Eq. 11) and photo-protection (Eqs. 12 and 13) based on the redox state of the Q_A^T pool. For the latter we found a direct proportionality between the amount of photo-protection and the acclimation state of the cells represented by the photosynthetic unit size (Fig. 7).

The light response of ETR—The most common formalism that oceanographers use to describe the light dependence of photosynthesis is the photosynthesis-light response (P-I) curve (MacIntyre et al. 2002). An alternative approach based on quantum-yield–light curves (Kiefer and Mitchel 1983; Sakshaug et al. 1989) has also been employed, particularly within the context of bio-optical models of primary productivity. The equivalence of these approaches can be readily demonstrated (Geider 1990). Plots of ETR_Q and ETR_C vs. photon flux density (Fig. 5a, c) show striking similarities to plots of chlorophyll- and carbon-specific photosynthesis rates against PFD (MacIntyre et al. 2002). Specifically, the initial slope of the ETR_Q vs. I and P_{chl} vs. I curves are largely independent of whether cells are acclimated to high or low light, whereas the light-saturated ETR_Q and P_{chl} are higher in cells

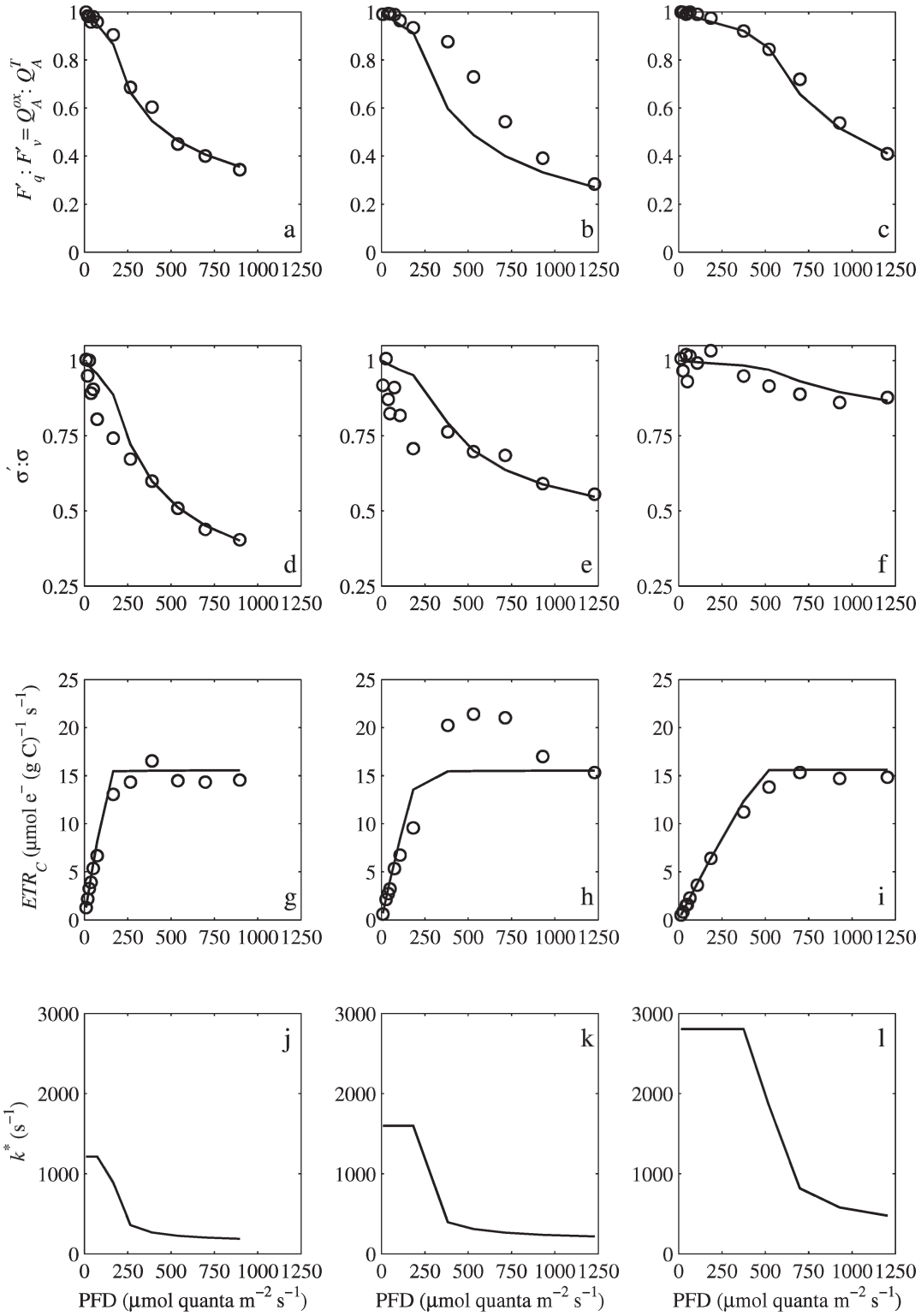

Fig. 6. Comparison between the model output (solid lines) and FRRF data (symbols) for (a, d, g, j) the LL culture with $\beta = 0.95$, (b, e, h, k) the ML culture with $\beta = 0.65$, and (c, f, i, l) the HL culture with $\beta = 0.25$. In frames (a), (b) and (c), the model predictions of $Q_A^{ox}:Q_A^T$ are shown together with estimates of this variable given FRR measurements of $F_q^{'}:F_v^{'}$. See Table **1** for the remaining parameter values. Photo-inhibition has been disabled for these plots (i.e., $\Psi_d = 0$).

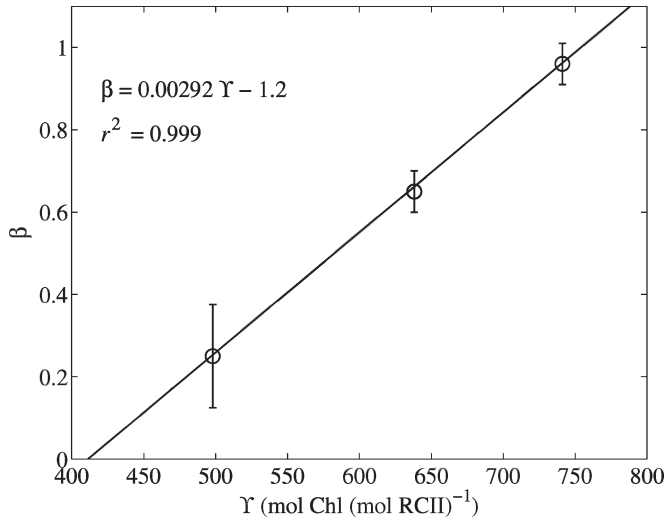

Fig. 7. Dependence of the amount of photo-protection (expressed through the parameter β) on the photosynthetic unit size Υ for *D. tertiolecta*. The values for β are chosen independently, such that the model reproduces the magnitude of the observed depression in $\sigma' : \sigma$ (*see* Fig. 6). It is expected that the fit constants are species dependent. The error bars are based on the possible range of values for β that still delivers acceptable fits to the data.

acclimated to high light. In contrast, the light-saturated carbon-specific *ETR*, $ETR_C^{\max}$, and the light-saturated carbon-specific photosynthesis rate, $P_C^{\max}$, are largely independent of whether cells are acclimated to high or low light, whereas the initial slopes of ETR_C vs. I or P_C vs. I curves decrease in high light. This strategy of acclimation allows for a decline in the C-specific rate of light absorption in high-light conditions through reductions of cell chlorophyll and RCII contents relative to cell carbon contents.

The dependence of ETR on Q_A redox state—When formulating our model, we hypothesized that the slope of a plot of ETR_Q vs. $Q_A^{red}:Q_A^a$ should be a constant (Fig. 2) that is determined by the maximum rate of electron transfer from Q_A^- to Q_B. We designated this slope $k_Q^{\max}$. Experimentally, we found that $k_Q^{\max}$ was not constant. Rather $k_Q^{\max}$ showed acclimation to the photon flux density at which the cells were grown (Fig. 5b). We also found that $k_Q^{\max}$ was correlated with $ETR_Q^{\max}$. In other words, the maximum rate of reoxidation of closed RCII reaction centers, $k_Q^{\max}$, depended on the photo-acclimation state in *D. tertiolecta*. The highest value of $k_Q^{\max}$ (2,800 s^{-1}) was obtained in cells acclimated to high light. This value is consistent with that expected for the transfer of an electron from Q_A^- to Q_B with an average e-folding time of about 375 μs. A much lower value of $k_Q^{\max}$ (1,200 s^{-1}) was calculated for cells acclimated to low light. This suggests that reoxidation of $Q^-{}_A$ in low-light cells was limited by reactions downstream of the transfer to Q_B, even when the Q_A pool was largely oxidized. The observed time constant for the reoxidation of Q_A^- is the result of the sequential reduction of Q_B to Q_B^- and Q_B^- to Q_B^{2-} (Falkowski and Raven 2007). The first reduction step has a time constant of about 150 μs whereas the second has a time constant of 600 μs (the mean of these two time constants is 375 μs). Thus, the time constant for reoxidation of Q_A^- will depend on whether the associated Q_B is oxidized or singly reduced. One possible explanation for the variability of $k_Q^{\max}$ that we observed (Fig. 5b) is that the relationship between Q_A^- and the redox state of Q_B, which is not included in our model, under actinic light depends on the photo-acclimation state of the cells. This in turn implies that the rate constant for exchange of Q_B^{2-} with plastoquinone decreases at low light. Variability in the rate constant for this exchange has been suggested to occur as a response to photo-inhibition in *Chlorella* (Kaňa et al. 2002).

Light harvesting in puddle and lake models—Light harvesting by PSII can be described as either a puddle or a lake (Govindjee 2004). In the puddle model, an exciton is absorbed by a discrete PSII antenna and can only visit the specific reaction center associated with this antenna, (i.e., all reaction centers are isolated from each other). In a lake model, the PSII reaction centers share a common antenna, and an exciton can freely migrate amongst them. In reality, the light harvesting by PSII is intermediate between a lake and a puddle: in this case the PSII are said to be connected, but the degree of connectivity can vary amongst taxa and with physiological condition (Falkowski and Raven 2007). Whether PSII in *Dunaliella* is organized as lakes or puddles (or has intermediate degrees of connectivity) has important implications for determining the average size of the antenna that is associated with a PSII reaction center, the relationship between light absorption and photochemistry, and the use of fluorescence to assess the redox state of Q_A (Kramer et al. 2004). Fortunately, the antenna organization of PSII does not affect the use of fluorescence to estimate photosynthetic electron transfer rates via Eq. 3. Although connectivity should be taken into account in calculating the redox state of Q_A from fluorescence (Kramer et al. 2004), the linear relationship between $F_q':F_v'$ and Q_A^{ox} that we assume in our calculations (Eq. 3) appears a reasonable approximation for *Dunaliella tertiolecta* in which the connectivity parameter, p, has a typical value of about 0.3.

Photo-inhibition and recovery—Our model, like those of Han (2002) and Baklouti et al. (2006) assumes that the function for photo-inactivation of PSII reaction centers depends on the rate of exciton delivery to the reduced reaction centers (e.g., to overexcitation of Q_A^{red}). This formulation is consistent with evidence summarized by Melis (1999) based largely on experiments done with the chlorophyte *Dunaliella salina*. This formulation is by no means universally accepted. There is considerable evidence indicating that RCII inactivation is proportional to the photon flux density, independent of the redox state of Q_A. Thus, a simpler model assumes that photo-inactivation of RCII is proportional to the rate of light absorption, consistent with data for vascular plant leaves (Anderson et al. 1998), the cyanobacterium *Synechocystis* (Allakhyverdiev et al. 2005) and even Melis' (1999) data for *Dunaliella salina*. In our model simulations (Fig. 6) we chose to exclude photo-inhibition because the FRRF data from

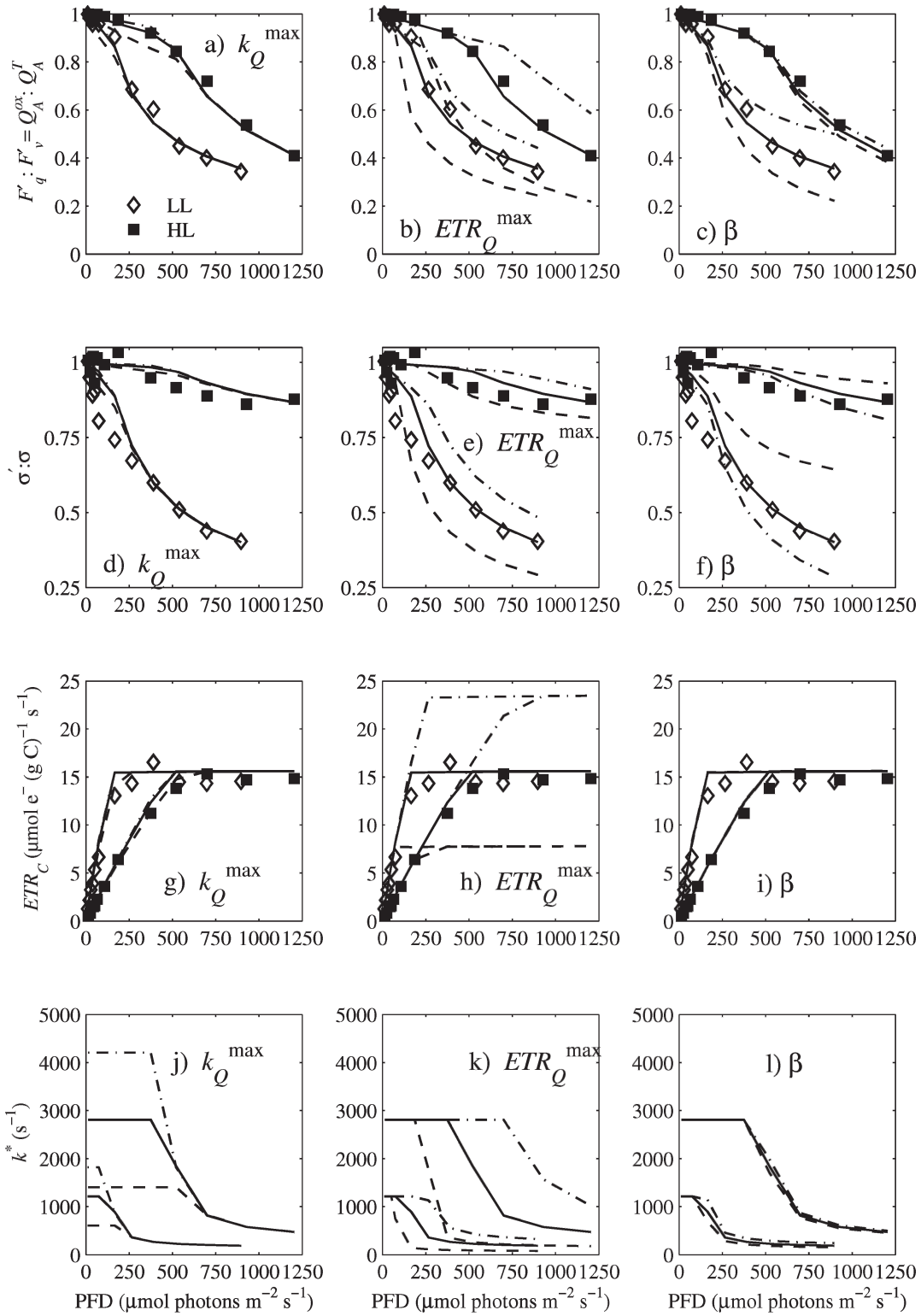

Fig. 8. Sensitivity of the model to changes in (a, d, g, j) k_Q^{max}, (b, e, h, k) ETR_Q^{max} and (c, f, i, l) β for the LL (open symbols) and the HL culture (filled symbols). The solid lines show the original model results with the values from Table 3. The dashed lines are for the parameter values −50% and the dash-dotted lines are for the parameter values +50%.

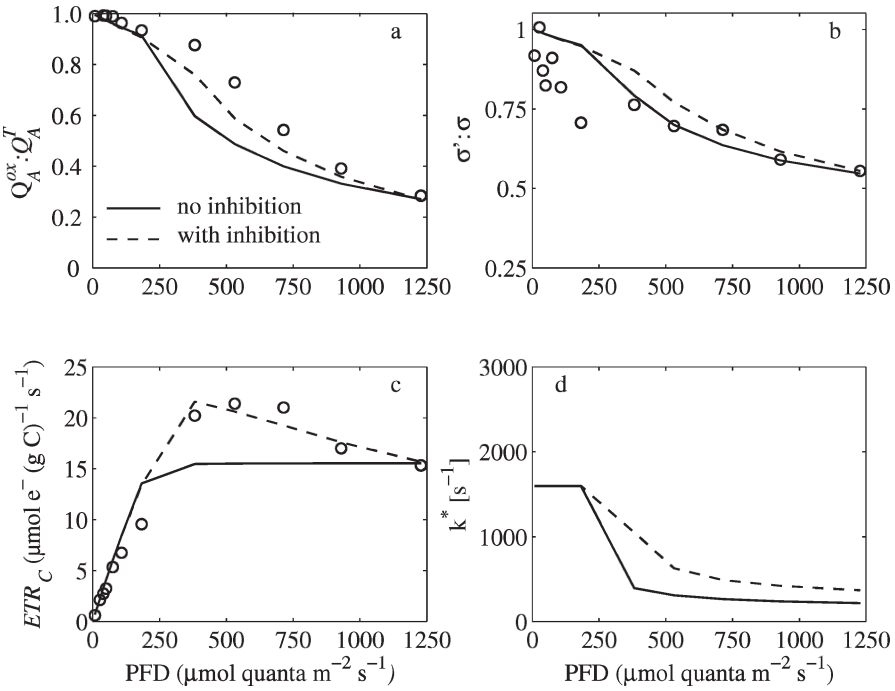

Fig. 9. Alternative model results to Fig. 6b, e, h, k where photo-inhibition has now been turned on and a higher value for $ETR_Q^{\max}$ is used ($\Psi_d = 1.6 \cdot 10^{-6}$ and $ETR_Q^{\max} = 229$ mol e$^-$ [mol RCII]$^{-1}$ s^{-1}).

both the low- (LL) and high-light (HL) cultures did not show any significant decrease in ETR at very high PFDs during the short exposure times. However, by including photo-inhibition, we can improve the fit to the data from the medium light (ML) culture which showed higher values of $ETR^{\max}$ at intermediate light intensities and a decrease towards the high PFDs. If we thus apply a higher value of $ETR^{\max}$ while allowing for photo-inhibition, the fit of the model to the data is considerably improved (Fig. 9). It is unclear, however, why the ML culture should exhibit photo-inhibitory behavior while the LL culture does not.

Photo-protection—The amount of photo-protection, β, is one of the two tuneable parameters of this model. Our comparison of β with the acclimation state of the cells expressed as the photosynthetic unit size Υ, yielded a striking relationship (Fig. 7) which suggests that β may be directly related to experimentally measured parameters. We did not investigate the mechanism responsible for the light dependence of σ' in *Dunaliella tertiolecta*. It is possible that a proportion of the reduction of σ' with increasing PFD is due to state-transitions, whereby excitation energy is redirected from RCII to RCI (Allen 2002). This hypothesis is consistent with the greater dependence of σ' on PFD in low-light than high-light acclimated conditions. Both the ratio of Chl *a*-to-RCII (Υ) and the value of the effective cross-section in darkness (σ) are larger in LL- than in HL-acclimated *D. tertiolecta*. Thus, there is greater potential for state-transition quenching in the LL culture, which is what we observe. Furthermore, both the PSII to PSI transition and the PSI to PSII transitions are mediated by the redox state of the PQ pool (Allen 2002). Similarly, Garcia-Mendoza et al. (2002) observed that NPQ was greater in low-light–acclimated *Chlorella fusca* than in high-light–acclimated cells. Furthermore, they observed that most of the NPQ in low-light cells was due to state transitions rather than the xanthophyll cycle (e.g., NPQ was little affected by dithiothreithol, an inhibitor of the xanthophyll cycle).

Photo-acclimation—In *D. tertiolecta*, as in other phytoplankton, the ratio of Chl *a*-to-carbon declines in cells as they acclimate to high light (Table 3). This reduces the rate of light absorption and, thus, the excitation pressure on the total pool of RCII. Reductions in light absorption relative to the rate of photosynthesis reduces the potential for photo-inhibitory damage (Melis 1999). The photosynthetic unit size, defined as the ratio of Chl *a* to Q_A^a, also declines during acclimation to high light in *D. tertiolecta* (Table 3) and other phytoplankton (Dubinsky et al. 1986). Again, this can be seen as a strategy that reduces the excitation pressure on RCII. The reduction of photosynthetic unit size is mechanistically responsible for a reduction in the effective cross-section of PSII (Table 3), and concomitant with changes in the ratio Q_A^a:C is an increase in both $k_Q^{\max}$ and $ETR_Q^{\max}$ (Fig. 5).

A number of steps are required before our model can be extended to include photo-acclimation of Chl *a*:C and Q_A^a:C. First, the dependence of the parameters σ, $k_Q^{\max}$, and $ETR_Q^{\max}$ on the state variables Q_A^a:C and Chl *a*:Q_A^a need to be established. Our data suggest that such relationships exist. For example, the degree of photo-protection was linearly related to photosynthetic unit size (Fig. 7), and σ was linearly related to Chl *a*:Q_A^a (Fig. 10) for *D.*

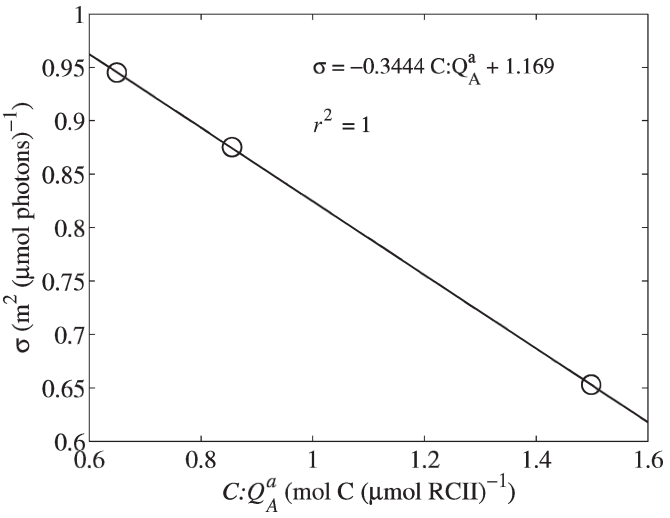

Fig. 10. Dependence of the PSII absorption cross-section, σ, on the acclimation state of the cultures (using data from Table 3).

tertiolecta in balanced growth. Given the assumptions of constant $ETR_C^{\max}$ and $k_C^{\max}$, $ETR_Q^{\max}$ and $k_Q^{\max}$ are linearly related to $(Q_A^a)^{-1}$.

In previous models of photo-acclimation of Chl *a*:C (Geider et al. 1998), it was assumed that the values of model parameters were determined by the ratios of state variables whether cells were in balanced growth or exposed to transient conditions. Having established the dependence of parameter values on state variables under conditions of balanced growth (Figs. 7, 10), we only need to specify a set of coupled differential equations to describe the rates of change of the state variables. The rate of change of organic carbon, C, is simply the difference between carbon-specific photosynthesis (P_C) and carbon-specific respiration (R_C) (Geider et al. 1998):

$$\frac{1}{C}\frac{dC}{dt} = P_C - R_C \tag{6}$$

Currently, there are several formulations available for acclimation of the Chl *a*-to-carbon ratio (Chl *a*:C) to choose from (Geider et al. 1998; Flynn 2001; Pahlow 2005). Finally, it will be necessary to develop an additional equation to describe the acclimation of photosynthetic unit size. There is strong evidence that photo-acclimation is regulated by a signal generated within the photosynthetic electron transfer chain, specifically by the redox state of the plastoquinone pool (Escoubas et al. 1995). One issue that must be addressed before photo-acclimation can be included in the model is how to represent this signal. Within our model, the possible signals are the redox state of Q_A and the relative size of the effective cross-section of PSII, $\sigma':\sigma$. In future research, we plan to explore the possibility of using Q_A^{ox}, Q_A^{red}, and $\sigma':\sigma$ as signals in differential equations describing the photo-acclimation of Chl *a*:C.

Comparison to ^{14}C—Since the introduction of the ^{14}C method by Steemann-Nielsen (1952), ^{14}C productivity measurements have been the primary data source that informs our knowledge of marine primary productivity (Barber and Hilting 2002). Validation of the FRR methodology for applications to marine primary productivity have rested on comparisons with results obtained using the ^{14}C method (e.g., Kolber and Falkowski 1993). Here we compare our model estimates of carbon-specific electron transfer rates, ETR_C, with carbon-specific carbon fixation rates measured by ^{14}C assimilation, P_C (Fig. 11). As described in the methods, ETR_C is based on the model output, which was calibrated with measurements made for 4 min at each of 13 PFDs, whereas P_C was based on 40-min incubations at each of 24 PFDs. The independent light response curves show extremely good agreement (Fig. 11). This comparison indicates that P_C is proportional to ETR_C, with the ratio of CO_2 assimilation to ETR being $\Phi_C = 0.111$. The reciprocal of Φ_C is the electron requirement for CO_2 fixation, which from Fig. 11 is 9 mol e^- (mol CO_2)$^{-1}$. This value is higher than expected. Based on the reductant required for CO_2 fixation into carbohydrate, we expect a ratio of 4 mol e^- (mol CO_2)$^{-1}$. This must be increased by the photosynthetic quotient to account for the additional reductant required for nitrate assimilation and biosynthesis of organic matter that is more reduced than carbohydrate (Kroon and Thoms 2006). A typical photosynthetic quotient for growth on nitrate is 1.5 mol O_2 (mol CO_2)$^{-1}$, raising the electron requirement to 6 mol e^- (mol CO_2)$^{-1}$. Thus, about one-third of the ETR_C (about 3 mol e^- [mol CO_2]$^{-1}$) is unaccounted for. Significantly, this mismatch applies at both light-limiting and light-saturating PFDs.

Several processes or errors may account for the difference between ETR_C and P_C that we observed. Systematic methodological errors that could lead to an overestimate of ETR include overestimating the photon flux density and/or the effective cross-section (σ'; *see* Eq. 10). A systematic methodological error that could result in underestimate of P_C is underestimation of the effect of isotope discrimination against ^{14}C relative to ^{12}C: the factor used in calculating P_C assumed a discrimination factor of 1.04. Although we cannot discount the possible individual or cumulative effects of such systematic methodological errors, we also need to look for photosynthetic (or respiratory) processes that could account for the mismatch.

There are at least five mechanisms that could account for the mismatch between ETR_C and ^{14}C assimilation. These are cyclic electron flow around RCII (Falkowski et al. 1986), reduction of O_2 at PSI as part of the water–water cycle (Asada 2000), photorespiratory O_2 consumption by the oxygenase activity of Rubisco (Miziorko and Lorimer 1983), chlororespiration (Peltier and Cournac 2002), and mitochodrial respiration of recent photosynthate (Weger et al. 1989). Most of these mechanisms have been hypothesized to increase the dissipation of excess energy at high light. As such, they cannot account for our observation of a constant ratio of ETR_C to P_C at all PFDs from light-limitation to light-saturation. Of these mechanisms, photorespiratory O_2 consumption could account for diversion of a constant proportion of NADPH from CO_2 fixation at all PFDs provided that the ratio of O_2 to CO_2 at the active site of Rubisco does not vary with PFD. That photorespiration may play a significant role in *D. tertiolecta* is indicated by

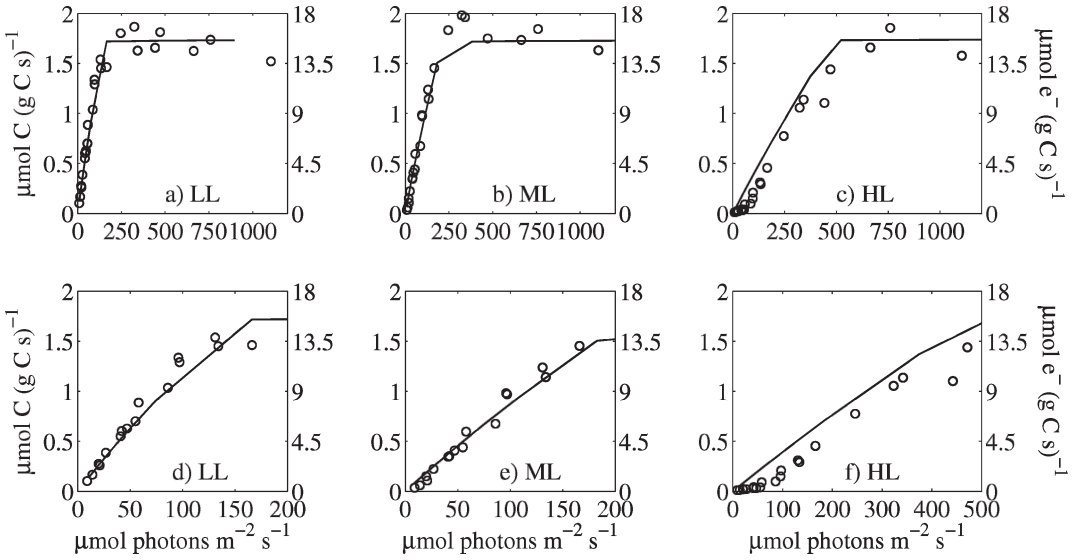

Fig. 11. Results from ^{14}C measurements (open symbols, left axes) on (a, d) the LL, (b, e) the ML, and (c, f) the HL culture. The solid lines (right axes) represent the model curves of ETR_C from Fig. 6.

high rates of light-dependent glyocate production observed in this alga (Leboulanger et al. 1998). Thus the only light-independent candidate for the uncoupling of ETR from ^{14}C fixation is photorespiration, but we do not have direct information to confirm this hypothesis.

Towards modeling the variability of quantum efficiency in the ocean—To infer primary productivity in the sea, we need to know the rate of light absorption by the phytoplankton and the quantum efficiency of photosynthesis. To a first approximation, the rate of light absorption depends on the incident photon flux density and the Chl *a* concentration, both of which can be measured in a variety of ways including satellite remote-sensing. Increases in accuracy of primary-productivity algorithms have been obtained by including information on the vertical light-attenuation coefficient, the vertical distribution of Chl *a* concentration and the Chl *a*–specific light-absorption coefficient. All of these factors affect the rate of light absorption by the phytoplankton.

Less easy to characterize than the underwater light and chlorophyll fields is the variability of the quantum efficiency of photosynthesis. However, the introduction of pump-and-probe (Kolber and Falkowski 1993) and fast repetition rate (Kolber et al. 1998) fluorometry provided methods for more accurately evaluating the spatial and temporal variability of the quantum efficiency of PSII photocehmistry. Consistent with this assertion are observations of co-variability between FRR-based estimates of *ETRc*, which rely on an estimate of quantum efficiency of PSII photocehmistry, and ^{14}C-fixation across ocean regions dominated by diatoms and dinoflagellates ($r^2 = 0.81$; Melrose et al. 2006) and by picophytoplankton ($r^2 = 0.90$; Corno et al. 2006). These methods promised to provide "not only a means of quantifying the variability in such key parameters as quantum yield" but also to permit "investigation of the relationship of the variability of phytoplankton photosynthesis to physics and chemistry of the ocean on matched time and space scales" (Kolber and Falkowski 1993).

Oceanographers are rapidly accumulating a database of observations of quantum efficiency of PSII based on FRR fluorescence. It is therefore appropriate to consider how to exploit this data base using dynamic models of phytoplankton photosynthesis. These models must be simple enough to be used in conjunction with physical models of ocean mixing, yet they must still capture essential processes that influence the rate of light absorption and quantum efficiency of phytoplankton photosynthesis. These processes include photosynthesis, photo-protection, photo-inhibition, and photo-acclimation. Development of these models requires appropriate data sets obtained under controlled conditions in the laboratory and at sea. In turn, these models can inform oceanographers about how to collect data using FRR fluorometry that will not only allow us to document the variability of the quantum efficiency of photosynthesis, but also to determine how phytoplankton adapt to and exploit the fluctuating light field in nature.

References

Allakhyverdiev, S. I., Y. Nashiyama, S. Takahashi, S. Miyairi, I. Suzuki, and N. Murata. 2005. Systematic analysis of the relation of electron transport and ATP synthesis to the photodamage and repair of photosystem II in *Synechocystis*. Plant Physiol. **137:** 263–273.

Allen, J. F. 2002. Plastoquinone redox control of chloroplast thylakoid protein phosphorylation and distribution of excitation energy between photosystems: Discovery, background, implications. Photosynth. Res. **73:** 139–148.

Anderson, J. M., Y.-I. Park, and W. S. Chow. 1998. Unifying model for the photoinactivation of photosystem II in vivo under steady-state photosynthesis. Photosynth. Res. **56:** 1–13.

Asada, K. 2000. The water–water cycle as alternative photon and electron sinks. Philos. Trans.: Biol. Sci. **355:** 1419–1431.

Baklouti, M., F. Diaz, C. Pinazo, V. Faure, and B. Queguiner. 2006. Investigation of mechanistic formulations depicting phytoplankton dynamics for models of marine pelagic ecosystems and description of a new model. Prog. Oceanogr. **71:** 1–33.

Barber, R. T., and A. K. Hilting. 2002. History of the study of plankton productivity, p. 16–43. *In* P. J. L. Willams, D. N. Thomas and C. S. Reynolds [eds.], Phytoplankton productivity: Carbon assimilation in marine and freshwater ecosystems. Blackwell.

Behrenfeld, M. J., O. Prasil, Z. S. Kolber, M. Babin, and P. G. Falkowski. 1998. Compensatory changes in photosystem II electron turnover rates protect photosynthesis from photoinhibition. Photosynth. Res. **58:** 259–268.

Bertoni, R., and E. Balseiro. 2005. Mixing layer running incubator (MIRI): An instrument for incubating samples while moving vertically in the mixing layer. Limnol. Oceanogr: Methods **3:** 158–163.

Corno, G., R. M. Letelier, M. R. Abbott, and D. M. Karl. 2006. Assessing primary production variability in the north Pacific subtropical gyre: A comparison of Fast Repetition Rate fluorometry and ^{14}C measurements. J. Phycol. **42:** 51–60.

Cullen, J. J. 1990. On models of photosynthesis in phytoplankton. Deep-Sea Res. **37:** 667–683.

———, and M. R. Lewis. 1988. The kinetics of algal photoadaptation in the context of vertical mixing. J. Plankton Res. **10:** 1039–1063.

Dera, J., and H. R. Gordon. 1970. Light field fluctuations in the photic zone. Limnol. Oceanogr. **13:** 697–699.

Dubinsky, Z., P. G. Falkowski, and K. Wyman. 1986. Light harvesting and utilization by phytoplankton. Plant Cell Physiol. **27:** 1335–1349.

Eilers, P. H. C., and J. C. H. Peeters. 1988. A model for the relationship between light intensity and the rate of photosynthesis in phytoplankton. Ecol. Model. **42:** 199–215.

Escoubas, J. M., M. Lomas, J. Laroche, and P. G. Falkowski. 1995. Light intensity regulation of cab gene transcription is signaled by the redox state of the plastoquinone pool. Proc. Natl. Acad. Sci. U. S. A. **92:** 10237–10241.

Falkowski, P. G., and J. A. Raven. 2007. Aquatic photosynthesis, 2nd ed. Princeton Univ. Press.

———, K. Wyman, A. C. Ley, and D. C. Mauzerall. 1986. Relationship of steady-state photosynthesis to fluorescence in eucaryotic algae. Biochim. Biophys. Acta **849:** 183–192.

Flynn, K. J. 2001. A mechanistic model for describing dynamic multi-nutrient, light, temperature interactions in phytoplankton. J. Plankton Res. **23:** 977–997.

Gallegos, C. L., G. M. Hornberger, and M. G. Kelly. 1977. A model of river benthic algal photosynthesis in response to rapid changes in light. Limnol. Oceanogr. **22:** 226–233.

Garcia-Mendoza, E., H. C. P. Matthijs, H. Schubert, and L. R. Mur. 2002. Non-photochemical quenching of chlorophyll fluorescence in *Chlorella fusca* acclimated to constant and dynamic light conditions. Photosynth. Res. **74:** 303–315.

Geider, R. J. 1990. The relationship between steady state phytoplankton growth and photosynthesis. Limnol. Oceanogr. **35:** 971–972.

———, H. L. MacIntyre, and T. M. Kana. 1996. A dynamic model of photoadaptation in phytoplankton. Limnol. Oceanogr. **41:** 1–15.

———, ———, and ———. 1998. A dynamic regulatory model of phytoplanktonic acclimation to light, nutrients, and temperature. Limnol. Oceanogr. **43:** 679–694.

Gocke, K., and J. Lenz. 2004. A new 'turbulence incubator' for measuring primary production in non-stratified waters. J. Plankton Res. **26:** 357–369.

Gorbunov, M. Y., Z. S. Kolber, M. P. Lesser, and P. G. Falkowski. 2001. Photosynthesis and photoprotection in symbiotic corals. Limnol. Oceanogr. **46:** 75–85.

Goss, R., B. Lepetit, and C. Wilhelm. 2006. Evidence for a rebinding of antheraxanthin to the light-harvesting complex during the epoxidation reaction of the violaxanthin cycle. J. Plant Physiol. **163:** 585–590.

Govindjee, 2004. Chlorophyll a fluorescence: A bit of basics and history, p. 1–42. *In* G. C. Papageorgiou and Govindjee [eds.], Chlorophyll a fluorescence: A signature of photosynthesis. Springer.

Guillard, R. R. L., and J. H. Ryther. 1962. Studies of marine planktonic diatoms. I. *Cyclotella nana* Hustedt and *Detonula confervacea* (Cleve). Can. J. Microbiol. **8:** 229–239.

Han, B.-P. 2002. A mechanistic model of algal photoinhibition induced by photodamage to photosystem-II. J. Theor. Biol. **214:** 519–527.

Harris, G. P. 1978. Photosynthesis, productivity and growth: The physiological ecology of phytoplankton. Arch. Hydrobiol. **10:** 1–171.

Huisman, J., and B. Sommeijer. 2002. Population dynamics of sinking phytoplankton in light-limited environments: Simulation techniques and critical parameters. J. Sea Res. **48:** 83–96.

Jassby, A. D., and T. Platt. 1976. Mathematical formulation of the relationship between photosynthesis and light for phytoplankton. Limnol. Oceanogr. **21:** 540–547.

Jeffrey, S. W., R. F. C. Mantoura, and S. W. Wright. 1997. Phytoplankton pigments in oceanography: Guidelines to modern methods. UNESCO.

Jewson, D. H., and R. B. Wood. 1975. Some effects on integral photosynthesis of artificial circulation of phytoplankton through light gradients. Verh. Internat. Verein. Limnol. **19:** 1037–1044.

Kaňa, R., D. Lazár, O. Prášil, and J. Nauš. 2002. Experimental and theoretical studies on the excess capacity of photosystem II. Photosynth. Res. **72:** 271–284.

Keller, M. D., R. C. Selvin, W. Claus, and R. R. L. Guillard. 1987. Media for the culture of oceanic ultraphytoplankton. J. Phycol. **23:** 633–638.

Kiefer, D. A., and B. G. Mitchel. 1983. A simple, steady state description of phytoplankton growth based on absorption cross section and quantum efficiency. Limnol. Oceanogr. **28:** 770–776.

Kirkpatrick, G. J., T. B. Curtin, D. Kamykowski, M. D. Feezor, M. D. Sartin, and R. E. Reed. 1990. Measurement of photosynthetic response to euphotic zone physical forcing. Oceanography **3:** 18–22.

Knap, A., A. Michaels, A. Close, H. Ducklow and A. Dickson [Eds.]. 1996. Protocols for the Joint Global Ocean Flux Study (JGOFS) core measurements. JGOFS Project Office, Report No. 19.

Kolber, Z., and P. G. Falkowski. 1993. Use of active fluorescence to estimate phytoplankton photosynthesis in situ. Limnol. Oceanogr. **38:** 1646–1665.

Kolber, Z. S., O. Prásil, and P. G. Falkowski. 1998. Measurements of variable chlorophyll fluorescence using fast repetition rate techniques: Defining methodology and experimental protocols. Biochim. Biophys. Acta **1367:** 88–106.

Kramer, D. M., T. J. Avenson, and G. E. Edwards. 2004. Dynamic flexibility in the light reactions of photosynthesis governed by both electron and proton transfer reactions. Trends Plant Sci. **9:** 349–357.

Kroon, B. M. A., and S. Thoms. 2006. From electron to biomass: A mechanistic model to describe phytoplankton photosynthesis and steady-state growth rates. J. Phycol. **42:** 593–609.

Leboulanger, C., V. Martin-Jezequel, C. Descolas-Gros, A. Sciandra, and H. J. Jupin. 1998. Photorespiration in continuous culture of *Dunaliella tertiolecta* (Chlorophyta): Relationships between serine, glycine, and extracellular glycolate. J. Phycol. **34:** 651–654.

Lewis, M. R., E. P. W. Horne, J. J. Cullen, N. S. Oakey, and T. Platt. 1984. Turbulent motions may control phytoplankton photosynthesis in the upper ocean. Nature **311:** 49–50.

———, and C. J. Smith. 1983. A small-volume, short-incubation time method for the measurement of photosynthesis as a function of incident irradiance. Mar. Ecol. Prog. Ser. **13:** 99–102.

Lohr, M., and C. Wilhelm. 2001. Xanthophyll synthesis in diatoms: Quantification of putative intermediates and comparison of pigment conversion kinetics with rate constants derived from a model. Planta **212:** 382–391.

Long, S. P., S. Humphries, and P. G. Falkowski. 1994. Photoinhibition of photosynthesis in nature. Annu. Rev. Plant Physiol. Plant Mol. Biol. **45:** 633–662.

MacIntyre, H. L., R. J. Geider, and R. M. McKay. 1996. Photosynthesis and regulation of rubisco activity in net phytoplankton from Delaware Bay. J. Phycol. **32:** 718–732.

———, T. M. Kana, T. Anning, and R. J. Geider. 2002. Photoacclimation of photosynthesis irradiance response curves and photosynthetic pigments in microalgae and cyanobacteria. J. Phycol. **38:** 17–38.

———, ———, and R. J. Geider. 2000. The effect of water motion on short-term rates of photosynthesis by marine phytoplankton. Trends Plant Sci. **5:** 12–17.

MacKenzie, T. D. B., and D. A. Campbell. 2005. Cyanobacterial aclimation to rapidly fluctuating light is constrained by inorganic carbon status. J. Phycol. **41:** 801–811.

Mallin, M. A., and H. W. Paerl. 1992. Effects of variable irradiance on phytoplankton productivity in shallow estuaries. Limnol. Oceanogr. **37:** 54–62.

Marra, J. 1980. Vertical mixing and primary production, p. 121–137. *In* P. G. Falkowski [ed.], Primary productivity in the sea. Plenum Press.

Melis, A. 1999. Photosystem-II damage and repair cycle in chloroplasts: What modulates the rate of photodamage in vivo? Trends Plant Sci. **4:** 130–135.

Melrose, D. C., C. A. Oviatt, J. E. O'Reilly, and M. S. Berman. 2006. Comparisons of fast repetition rate fluorescence estimated primary production and 14C uptake by phytoplankton. Mar. Ecol. Prog. Ser. **311:** 37–44.

Miziorko, H. M., and G. H. Lorimer. 1983. Ribulose-1,5-bisphosphate carboxylase-oxygenase. Annu. Rev. Biochem. **52:** 507–535.

Mouget, J.-L., J. de al Noüe, L. Legendre, Y. Jean, and P. Viarouge. 1995*a*. Long-term acclimatization of *Scenedesmus bicellularis* to high-frequency intermittent lighting (100 Hz). I. Growth, photosynthesis and photosystem II activity. J. Plankton Res. **17:** 859–874.

———, L. Legendre, and J. de al Noüe. 1995*b*. Long-term acclimatization of Scenedesmus bicellularis to high-frequency intermittent lighting (100 Hz). II. Photosynthetic pigments, carboxylating enzymes and biochemical composition. J. Plankton Res. **17:** 875–890.

Olaizola, M., J. La Roche, Z. Kolber, and P. G. Falkowski. 1994. Non-photochemical fluorescence quenching and the diadinoxanthin cycle in a marine diatom. Photosynth. Res. **41:** 357–370.

Pahlow, M. 2005. Linking chlorophyll-nutrient dynamics to the Redfield N:C ratio with a model of optimal phytoplankton growth. Mar. Ecol. Prog. Ser. **287:** 33–43.

Peltier, G., and L. Cournac. 2002. Chlororespiration. Annu. Rev. Plant Biol. **53:** 523–550.

Platt, T., C. L. Gallegos, and W. G. Harrison. 1980. Photoinhibition of photosynthesis in natural assemblages of marine phytoplankton. J. Marine Res. **38:** 687–701.

Randall, J. M., and J. W. Day. 1987. Effects of river discharge and vertical circulation on aquatic primary production in a turbid Louisiana (USA) estuary. Neth. J. Sea Res. **21:** 231–242.

Raven, J. A., and R. J. Geider. 2003. Adaptation, acclimation and regulation in algal photosynthesis, p. 385–412. *In* A. W. D. Larkum, S. Douglas and J. A. Raven [eds.], Photosynthesis of algae. Kluwer Academic.

Ross, O. N., and J. Sharples. 2004. Recipe for 1-D Lagrangian particle tracking models in space-varying diffusivity. Limnol. Oceanogr.: Methods **2:** 289–302.

———, and ———. 2007. Phytoplankton motility and the competition for nutrients in the thermocline. Mar. Ecol. Prog. Ser. **347:** 21–38.

Sakshaug, E., K. Andresen, and D. A. Kiefer. 1989. A steady state description of growth and light absorption in the marine planktonic diatom *Skeletonema costatum*. Limnol. Oceanogr. **34:** 198–205.

Shoaf, W. T., and B. W. Lium. 1976. Improved extraction of chlorophyll a and b from algae using dimethyl sulfoxide. Limnol. Oceanogr. **21:** 926–928.

Smyth, T. J., K. L. Pemberton, J. Aiken, and R. J. Geider. 2004. A methodology to determine primary production and phytoplankton photosynthetic parameters from fast repetition rate fluorometry. J. Plankton Res. **26:** 1337–1350.

Steele, J. H. 1962. Environmental control of photosynthesis in the sea. Limnol. Oceanogr. **7:** 137–150.

Steemann-Nielsen, E. 1952. The use of radioactive carbon (C14) for measuring organic carbon production in the sea. J. du Conseil **18:** 117–140.

Stramski, D., G. Rosenberg, and L. Legendre. 1993. Photosynthetic and optical properties of the marine chlorophyte *Dunaliella tertiolecta* grown under fluctuating light caused by surface-wave focusing. Mar. Biol. **115:** 363–372.

Suggett, D. J., S. C. Maberly, and R. J. Geider. 2006. Gross photosynthesis and lake community metabolism during the spring phytoplankton bloom. Limnol. Oceanogr. **51:** 2064–2076.

———, H. L. MacIntyre, and R. J. Geider. 2004. Evaluation of biophysical and optical determinations of light absorption by photosystem II in phytoplankton. Limnol. Oceanogr.: Methods **2:** 316–332.

———, K. Oxborough, N. R. Baker, H. L. MacIntyre, T. M. Kana, and R. J. Geider. 2003. Fast repetition rate and pulse amplitude modulation chlorophyll a fluorescence measurements for assessment of photosynthetic electron transport in marine phytoplankton. Eur. J. Phycol. **38:** 371–384.

Sukenik, A., J. Bennett, and P. Falkowski. 1987. Light-saturated photosynthesis—limitation by electron transport or carbon fixation? Bioch. Biophys. Acta **891:** 205–215.

Wagner, H., T. Jakob, and C. Wilhelm. 2006. Balancing the energy flow from captured light to biomass under fluctuating light conditions. New Phytol. **169:** 95–108.

Weger, H. G., R. Herzig, P. G. Falkowski, and D. H. Turpin. 1989. Respiratory losses in the light in a marine diatom—measurements by short-term mass spectrometry. Limnol. Oceanogr **34:** 1153–1161.

Welschmeyer, N. A. 1994. Fluorometric analysis of chlorophyll a in the presence of chlorophyll b and phaeopigments. Limnol. Oceanogr. **39:** 1985–1992.

Wilhelm, C., and others. 2006. The regulation of carbon and nutrient assimilation in diatoms is significantly different from green algae. Protist **157:** 91–124.

Yoder, J. A., and S. S. Bishop. 1985. Effects of mixing-induced irradiance fluctuations on photosynthesis of natural assemblages of coastal phytoplankton. Mar. Biol. **90:** 87–93.

Zonneveld, C. 1997. Modeling effects of photoadaptation on the photosynthesis–irradiance curve. J. Theor. Biol. **186:** 381–388.

Received: 15 November 2007
Accepted: 14 March 2008
Amended: 8 April 2008